Fractional derivatives for the core losses prediction: State of the art and beyond

Benjamin Ducharne, Gaël Sebald

Fractional derivatives for the core losses prediction: state of the art and beyond

B. Ducharne, G. Sebald

ELyTMaX IRL3757, Univ Lyon, INSA Lyon, Centrale Lyon, Université Claude Bernard Lyon 1, Tohoku University, Sendai, Japan.

Abstract — The core losses prediction in laminated magnetic circuits has generated relentless scientific research efforts. In this domain, the almost forty years old Statistical Theory of Losses (STL) is still prevailing. Modern electrical energy conversion exposes laminated magnetic circuits to higher frequencies and larger excitation fields. STL, which requires a full flux penetration, poorly considered these intense stimuli. Recent studies proposed upgrading STL by modifying the classical eddy current loss term using fractional derivative operators. Excellent predictions were observed, but the lumped aspect inherent to STL means working with averaged quantities which constitutes a limitation. Alternatively, local predictions and good simulation trajectories were obtained for the frequency dependence of hysteresis by replacing the classic magnetic diffusion equation with a fractional one. Still, the physical origin of the fractional diffusion equation remains questionable. In the light of these results, we propose in this new study to review the use of the fractional derivative operators for the core losses prediction. We eventually revealed an alternative way to combine the classic diffusion equation to a fractional material law, leading to the ultimate fractional method, with physical fundaments, few parameters, and accurate results on significant frequency bandwidths.

Index Terms—Magnetic hysteresis, power converter, diffusion equation, fractional derivative, frequency effect, electrical steel.

I. INTRODUCTION

The magnetic core losses in electromagnetic devices have been studied for years [1]. It is a critical aspect of a new prototype design as these losses highly affect the conversion efficiency and the temperature distribution. Progress in this domain has been constant, fueled by the evolution of knowledge, technology, and instrumentation. Even if the first study on this topic was exposed in the early 20th century [1][2], the list of recent publications is remarkably long [3]-[7]. A plausible explanation for this surge of interest is the evolution of electromagnetic devices: faster, compacter, and more efficient, pushing the magnetic materials towards unprecedented working conditions (10 kHz in [5]). The hysteresis cycle is the standard magnetic signature of a magnetic core. It gives access to essential information, including coercivity, permeability, and the energy losses W [8]-[10]. The latter expressed in J·m^{-3} is equal to the $B_a(H_{surf})$ hysteresis cycle area (where B_a is the magnetic flux density and H_{surf}, the surface tangent magnetic excitation field). One well-known empirical equation to evaluate W in ferromagnetic electric steel laminations traces back to the original work of Steinmetz [11] more than a century ago. It is expressed with a scaling relation:

$$W = \kappa \cdot f^{\alpha} \cdot {B_{a_p}}^{\beta} \tag{1}$$

Where f and B_{ap} stand respectively for the frequency and the maximum induction. κ, α, and β are known as the Steinmetz coefficients. In Eq. 1, both exponents are non-integer numbers ($1 < \beta < 3$, $2 < \alpha < 3$ [12]-[14]), foreshadowing the use of non-integer operators for W's accurate simulations. In Steinmetz's publication, α and β are estimated empirically for every value of f and B_{a_p}. Unfortunately, this pragmatic approach shows limited predictive capability. Many years

later, Bertotti et al. described the Statistical Theory of Losses (STL) [15][16], introducing the concept of losses separation and leading to Eq. (2):

$$W = W_{hy} + W_{cl} + W_{ex} \tag{2}$$

Where, W_{hy} is the hysteresis loss contribution. W_{hy} is frequency-independent and related to elementary domain wall motions occurring at a microscopic scale. W_{hy} depends on the grain size, the texture, and the distribution of the precipitates. W_{cl} is the classical eddy current loss term. W_{cl} is the only contribution that would arise in a perfectly homogeneous material (no magnetic domain). W_{cl} is derived from Maxwell's equations and can be written as:

$$W_{cl} = \frac{\sigma d^2}{12} \cdot \int_0^{1/f} \left(\frac{dB_a}{dt}\right)^2 dt \tag{3}$$

σ is the electrical conductivity and d the magnetic sheet thickness. The last term W_{ex} is the excess loss. W_{ex} is a dynamic contribution related to the magnetic domains' kinetic and frequency dependency.

$$W_{ex} = \sqrt{\sigma S G V_0} \cdot \int_0^{1/f} \left|\frac{dB_a}{dt}\right|^{1.5} dt \tag{4}$$

$G = 0.1356$ is a dimensionless coefficient, S the cross-section area, and V_0 a max(B_a) dependent statistical parameter associated with the microstructure. STL is an efficient tool for predicting ferromagnetic losses. It is still widely used, especially for Oriented Grains electrical steel (FeSi GO) laminated sheets. However, STL was set assuming full magnetic field penetration and no skin effect; thus, its domain of validity remains limited to a few hundred hertz [17]. A few years later, core loss predictions were improved by abandoning the lumped relations and replacing them with space discretized methods. The 1D resolution of combining the magnetic field diffusion

equation Eq. (5) for the classic loss contribution and a viscosity-based magneto-dynamic model for both the hysteresis and the excess one gave the best results [18]. For this material law, a basic expression Eq. (6) can lead to a robust formulation Eq. (7) naturally solved by matrix inversion [19]:

$$\nabla^2 \mathrm{H} = \sigma \cdot \frac{\mathrm{dB}}{\mathrm{dt}} \tag{5}$$

$$\rho \cdot \frac{\mathrm{dB}}{\mathrm{dt}} = \mathrm{H} - \mathrm{H}_{\mathrm{stat}}(\mathrm{B}) \tag{6}$$

$$\nabla^2 \mathrm{H} = \sigma \cdot \frac{\mathrm{H} - \mathrm{H}_{\mathrm{stat}}(\mathrm{B})}{\rho} \tag{7}$$

Here, B and H are local quantities. ρ is a constant depending on the tested specimen's nature and geometry [20]. Unfortunately, for this simple approach, the frequency dependency of the excess losses is not taken into account appropriately, and overestimations can be observed in the high-frequency range. Much better results are obtained with Eq. (8) [21]:

$$\frac{\mathrm{dB}}{\mathrm{dt}} = \frac{\delta}{\mathrm{g(B)}} \cdot |\mathrm{H} - \mathrm{H}_{\mathrm{stat}}(\mathrm{B})|^{\alpha(\mathrm{B})} \tag{8}$$

Where δ is a directional parameter (= +/- 1) and the B dependent functions $\alpha(\mathrm{B})$ and $\mathrm{g}(\mathrm{B})$ are set by comparison with experimental results. Such a high number of parameters ends up with excellent simulation results but requires a significant amount of experimental data, which is complex to obtain in an industrial environment.

II. THEORITICAL CONSIDERATION

In this context of frequency limitation or over-sophisticated approaches, the demand for alternative techniques still exists. In light of this, new methods arose based on mathematical operators gathered from the framework of the fractional derivatives. Different methodologies have already been tested, including fractional differential equations [22][23]. Both the classic Preisach and Jiles-Atherton quasi-static hysteresis models $\mathrm{H_{stat}(B)}$ have been extended to the frequency dependence through the consideration of a fractional viscoelastic-type dynamic term:

$$\rho \cdot \frac{\mathrm{d^n B_a}}{\mathrm{dt^n}} = \mathrm{H_{surf}} - \mathrm{H_{stat}(B)} \tag{9}$$

Where n is the fractional order. Hybrid solutions have also been proposed, like in [24], where STL was partially modified. Authors obtained accurate simulation results on a significant frequency bandwidth, assuming the skin effect as solely affecting $\mathrm{W_{cl}}$ and replacing its usual expression with a fractional derivative one:

$$\mathrm{W = W_{hy} + W_{cl} + W_{ex} = \oint_l \left[H_{dy}(B_a)\right] dB_a} \tag{10}$$

$$\mathrm{H_{dyn} = H_{hy} + H_{cl} + H_{ex}} \tag{11}$$

$$\mathrm{W = \oint_l \left[H_{hy}(B_a) + H_{cl}(B_a) + H_{ex}(B_a)\right] dB_a} \tag{12}$$

$$\mathrm{W = \oint_l \left[H_{hy}(B_a) + \rho \cdot \frac{d^n B_a}{dt^n} + \sqrt{\sigma SGV_0} \cdot \delta \cdot \left|\frac{dB_a}{dt}\right|^{0.5}\right] dB_a} \tag{13}$$

This method provides precise losses estimation and works with a limited number of parameters, but, like the original STL, local information is not accessible. Even if the macroscopic eddy currents are taken into account, the distribution of H and B through the specimen cross-section remains unknown. The anomalous fractional diffusion equation is another option that seems to provide satisfactory results on a large frequency bandwidth:

$$\nabla^2 \mathrm{H} = \sigma' \cdot \frac{\mathrm{d}^n \mathrm{B}}{\mathrm{d}t^n} \tag{14}$$

In [25], this equation is solved in 1D for a laminated electrical steel sheet and 2D in [26] for a massive toroidal ferromagnetic core. In these publications and for energetical reasons, the fractional order is limited to the [0 – 1] range [27][28]. In Eq. (13), a decrease of n reduces the dynamic of the magnetic field diffusion, and for a given frequency f under sinus $\mathrm{B_a}$ imposed condition, it minimizes the losses. This observation is crucial as it somehow leads to an inconsistency in the low-frequency range where STL provides correct simulation results. The simultaneous consideration of the classic and excess losses by the anomalous fractional derivative equation means that accurate simulation results in the low-frequency range can only be obtained by over-estimating the pseudo electrical conductivity σ'. Fractional derivatives provide flexibility to the simulation method, allowing correct fittings on significant frequency bandwidths, but limitation remains:

- the lumped methods described in [21]-[23] are accurate but limited to average information.
- The anomalous fractional diffusion equation defined in [25]-[27] gives local information, but its physical meaning is questionable, and correct simulation results mean inaccurate electrical conductivity.

In light of these first observations, we propose in this work to further review the use of the fractional derivative operators for the loss prediction, conclude based on comparison criteria, and describe an ultimate fractional technique solving all the issues listed above while conserving excellent accuracy.

III. THE FRACTIONAL DERIVATIVE CALCULATION

Fractional Calculus (FC) is not new, and the first documents mentioning this branch of mathematics were published at the end of the seventeen century [28][29]. However, it is only recently that FC abandoned a purely mathematical perspective and started to generate interest in the applied science and engineering community [30][31]. FC can now be found in domains as diverse as biology, finance, or even signal processing [32]-[34]. FC shines by its faculty to simulate correctly long memory and long-range processes [35]. This non-locality in space and time can be observed in many phenomena, including fractional spaces [36], abnormal porous media [37], viscoelasticity [38], and diffusion processes [39]. Both the latter can specifically find an echo in the dynamical behavior of the magnetization processes described in this manuscript. Space fractional derivatives are recommended for the consideration of diffusion non-locality, which in other words, means to give a dependence of a local derivative result to every node of the discretized geometrical space [40]. These operators can be used with success to modulate the speed of the diffusion process according to the space position, the diffusion direction, and orientation. In the context of the magnetization process, where the electrical conductivity is supposed to be constant and isotropic, such operators are of limited interest. Time fractional derivatives are suggested in the context of long-time heavy tail decays, which involve the totality of the history in resolving a time derivative. Time fractional derivatives are well suited to ferromagnetic hysteresis, in which real-time behavior is strongly dependent on the specimen history. Derivatives in the time domain must respect the causality principle, a backward definition of decreasing time variation exists but doesn't match our experimental situation. This study limits

the time-fractional derivative definitions to a forward context. Eq. (15) gives the forward Grünwald-Letnikov expression:

$$\begin{cases} D_f^n f(t) = \lim_{h\to 0^+} h^{-n} \cdot \sum_{m=0}^{\infty} \frac{(-n)_m}{m!} \cdot f(t-mh) \\ (n)_m = \frac{\Gamma(n+m)}{\Gamma(n)} = m \cdot (m+1) \cdot \dots (n+m-1) \\ (m)_0 = 1 \end{cases} \quad (15)$$

Where $(n)_m$ is known as the Pochhammer symbol and Γ the gamma function. Eq. (15) exhibits multiple interesting properties [35], including:

- linearity
- additivity and commutativity
- neutral and inverse elements
- backward compatibility

If $f(\cdot)$ can be Laplace or Fourier transformed, its time-fractional derivative can also be expressed through an integral. The forward regularized Liouville derivative Eq. (16) is the integral form of Eq. (15) [35].

$$D_f^n f(t) = \frac{1}{\Gamma(-n)} \cdot \int_0^{\infty} \left[f(t-\tau) - u(n) \cdot \sum_0^{N-1} \frac{(-1)^m f^{(m)}(t)}{m!} \cdot \tau^m \right] \cdot \tau^{-n-1} d\tau \quad (16)$$

Where $u(\cdot)$ is the unit step function. The Liouville expression (Eq. (17)) is another fractional derivative definition that can be interpreted in terms of convolution between $f(t)$ and $t^n \cdot u(t)/\Gamma(1\text{-}n)$ [41].

$$D^n f(t) = \frac{1}{\Gamma(1-n)} \cdot \frac{d}{dt} \cdot \int_{-\infty}^{t} (t-\tau)^{-n} \cdot f(\tau) \cdot d\tau \quad (17)$$

$$(-\infty < t < +\infty)$$

In this study, both the Grünwald-Letnikov and the Riemann-Liouville were tested, and close simulation results and performances were observed.

IV. THE FRACTIONAL DERIVATIVE AS A TOOL FOR THE SIMULATION OF MAGNETIC LOSSES

Higher frequencies are promoted by the latest technological developments in the electrical energy conversion domain. Traditional magnetic core loss predictive methods have not been designed for high-frequency levels and show limitations. An ideal scenario would be accurate on a large frequency bandwidth, with physical meaning, few parameters, and local information. These criteria are listed in Table 1.

TABLE I

Core loss simulation method comparison criteria and simulation objectives.

Comparison criteria
Core losses under a harmonic regime
Core losses under arbitrary signals and transient regime
Spatial distribution (Skin effect)

Methods using time-fractional derivative operators show good potential. They are reviewed in this section.

A. The fractional differential equation method

The quasi-static Hysteresis losses W_{hy} are observed in the low-frequency range. They are due to domain wall motions of dynamical behaviors decorrelated to the excitation one. A good

estimation of this contribution can be obtained by assuming these domain wall motions act like mechanical dry-frictions [42][43]. For higher frequencies, these dry frictions turn to become viscoelastic, and $\rho \cdot dB_a/dt$ (equivalent to a lossy viscous damper, Eq. (6) is the typical additional contribution to take into account this change. Fig. 2 – c depicts the linear frequency dependency of the loss as obtained by solving Eq. (6) in sinus B_a imposed conditions (max(B_a) = 1.5 T). The quasi-static contribution (Fig. 1) comes from the J-A^{-1} model [44], and its parameters in Table 2 are set to match the magnetic answer of a typical FeSi GO [45]. Fig. 1 – a shows centered cycles, and Fig. 1 – b W_{hy} as a function of max(B_a).

TABLE II

J-A^{-1} parameters for a typical FeSi GO laminated electrical steel sheet.

J-A^{-1} Parameters	**Typical value**
a (A m^{-1})	4.4
Ms (A m^{-1})	1.41 10^6
k (A m^{-1})	13
c	0.42
α	9.8 10^{-6}

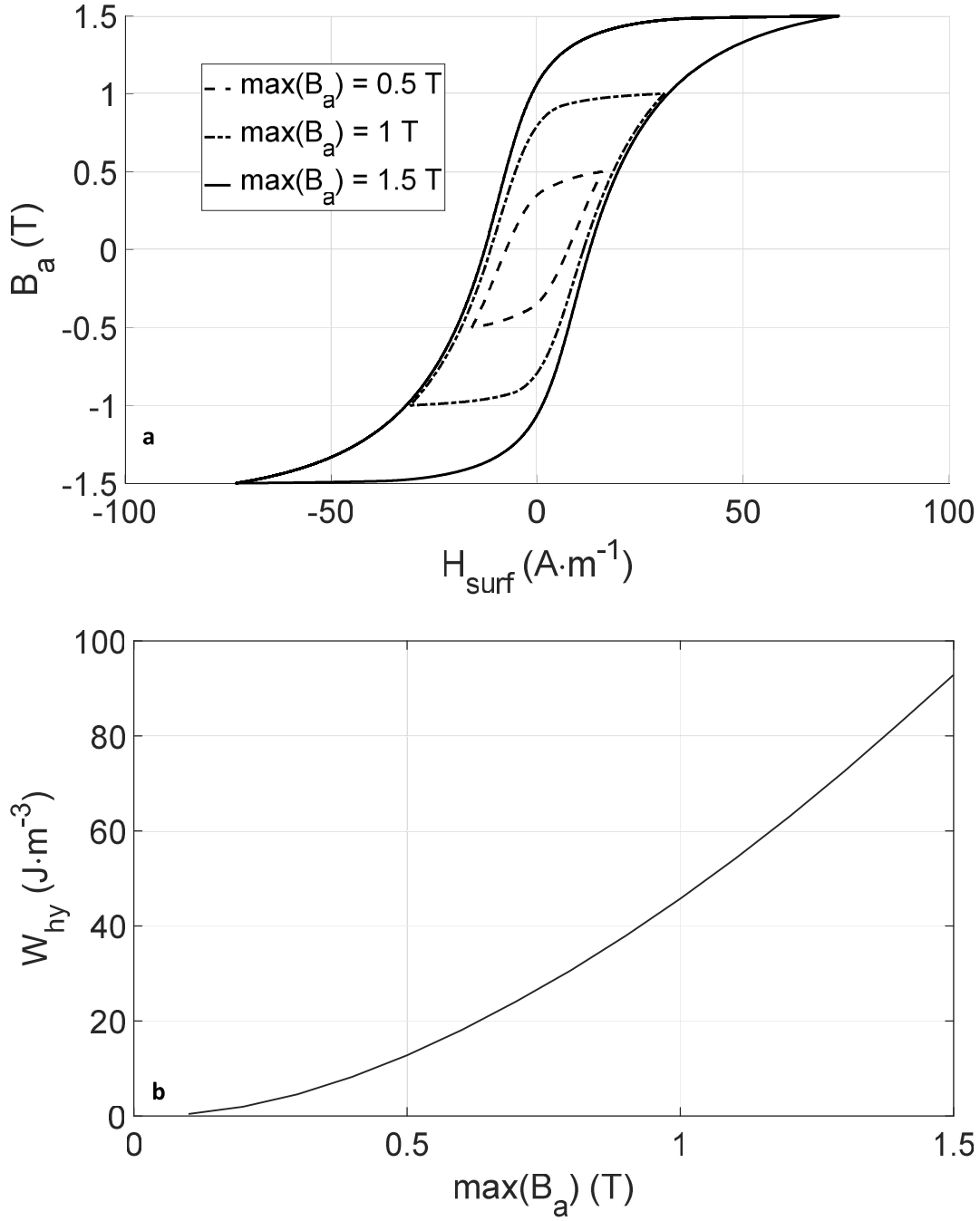

Fig. 1.a Quasi-static $B_a(H_{surf})$ hysteresis centered cycles simulation under sinus B_a imposed conditions using the J-A^{-1} model and the parameters depicted in Table 2. **Fig. 1.b** W_{hy} as a function of max(B_a) in the same conditions.

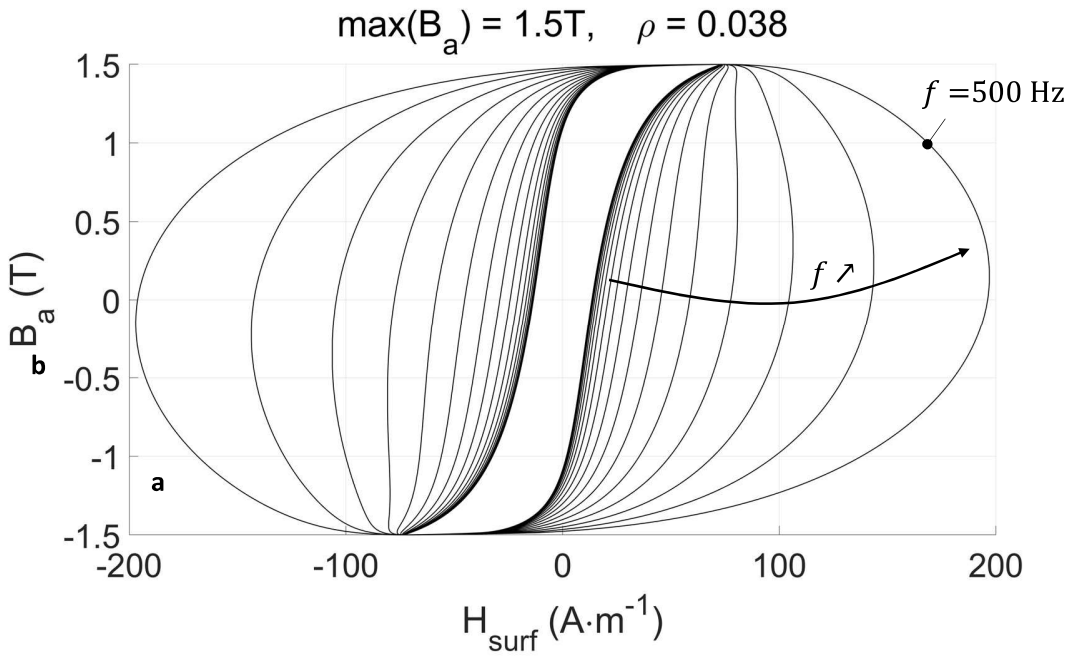
max(B_a) = 1.5T, ρ = 0.038
f =500 Hz
f ↗
B_a (T)
H_surf (A·m^-1)
a
b

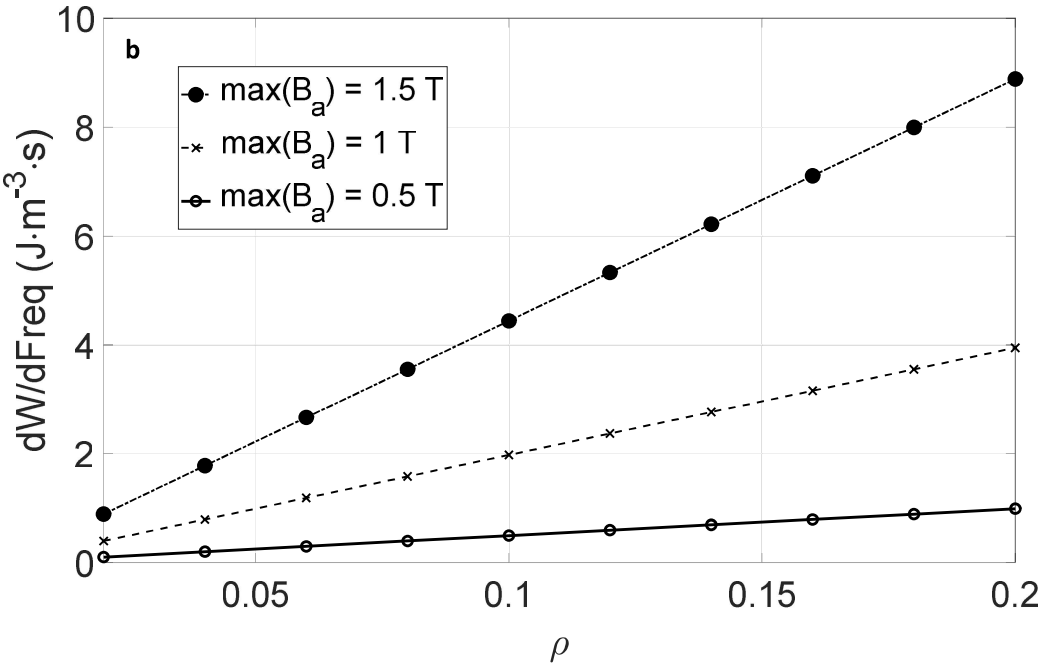
b
max(B_a) = 1.5 T
max(B_a) = 1 T
max(B_a) = 0.5 T
dW/dFreq (J·m^-3·s)
ρ

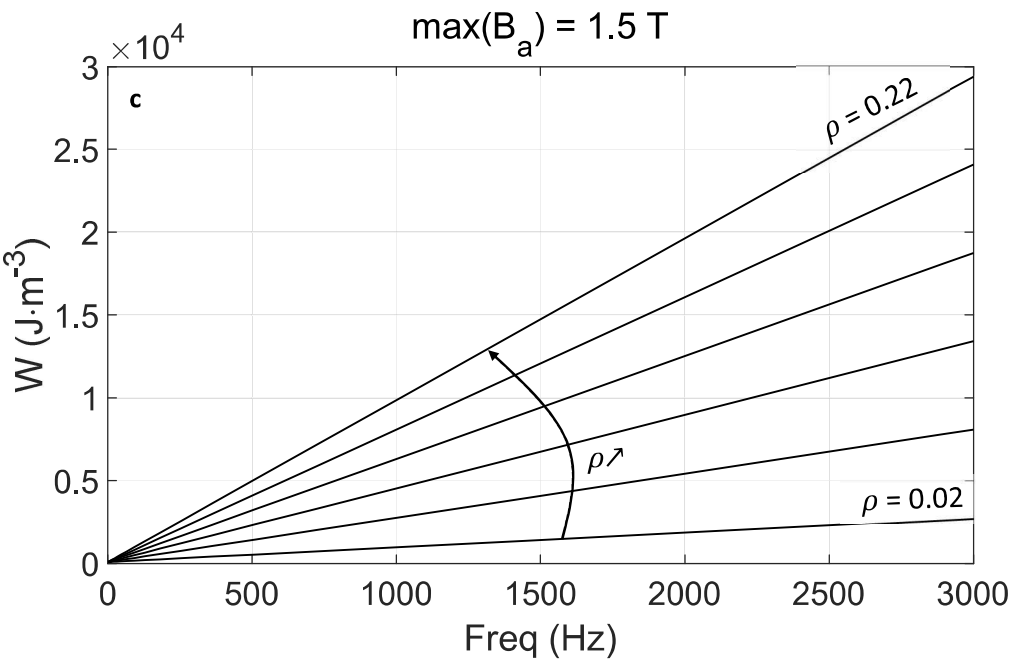

Fig. 2.a Hysteresis $B_a(H_{surf})$ cycles under increasing f as simulated with Eq. 5. **Fig. 2.b** dW/df as a function of ρ. **Fig. 2.c** Hysteresis core losses prediction, solving Eq. 5 under sinus flux density imposed conditions and max(B_a) = 1.5 T.

Fig . 2 – a shows some Eq. (6) $B_a(H_{surf})$ hysteresis cycles for increasing f, and Fig. 2 – b illustrates that for a given max(B_a), Eq. (6) leads to a dW/df proportional to ρ. As observed in Fig. 2 – c, $\rho \cdot dB_a/dt$ gives a linear frequency dependence of W, and ρ sets the slope. However, the experimental observations are far from linear, limiting the viability of Eq. (6) to a modest frequency bandwidth. $\rho \cdot d^n B_a/dt^n$ is the alternative solution proposed in [22][23]. The first-order derivative viscoelastic term is converted to a fractional one, and Eq. (9) becomes a fractional differential equation. Eq. (9) is easy to solve in sinus B_a imposed conditions as the fractional derivatives of harmonic functions have analytical solutions (Eq. 18, 19):

$$f(t) = e^{iat} \tag{18}$$

$$D_f^n f(t) = a^n \cdot \left(\cos\left(at + n\frac{\pi}{2}\right) + i\sin\left(at + n\frac{\pi}{2}\right)\right) \tag{19}$$

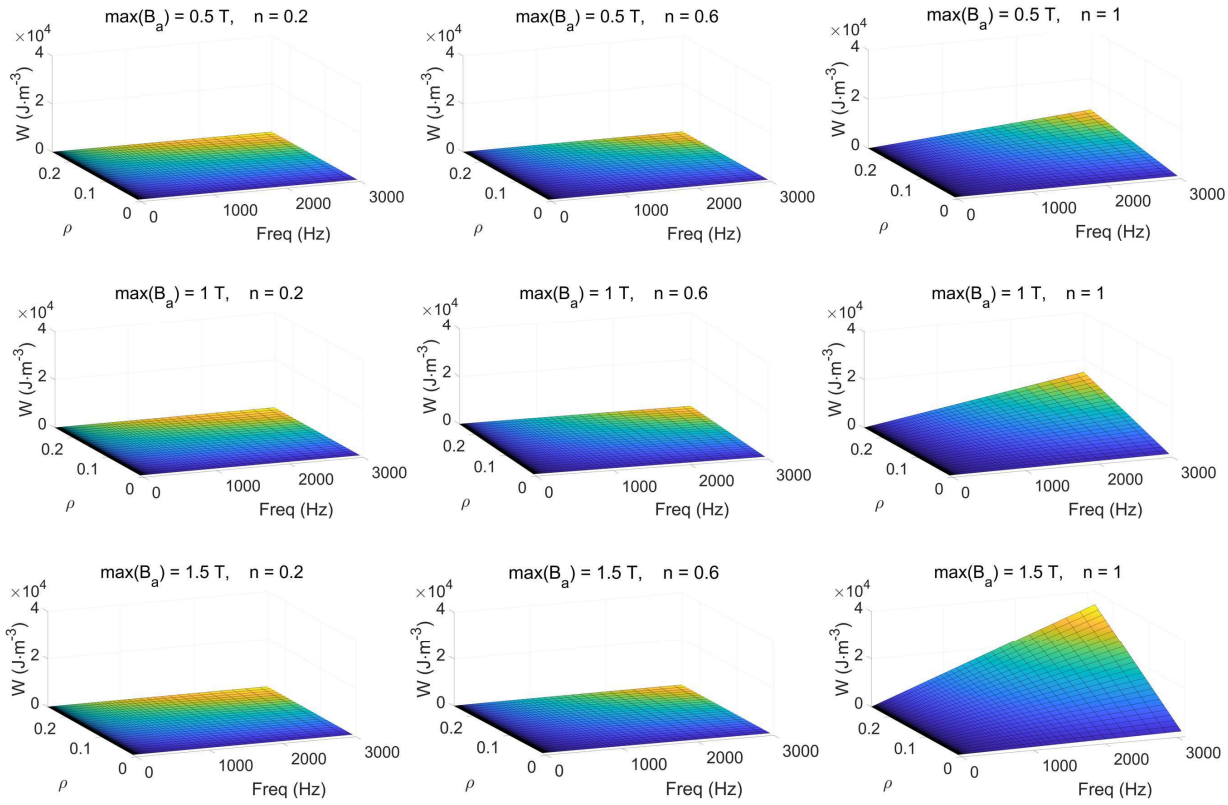

Fig. 3 Hysteresis core losses W simulation under sinus B_a imposed condition using the fractional viscoelastic differential equation (Eq. (9)) and increasing values of ρ, f, n, and max(B_a).

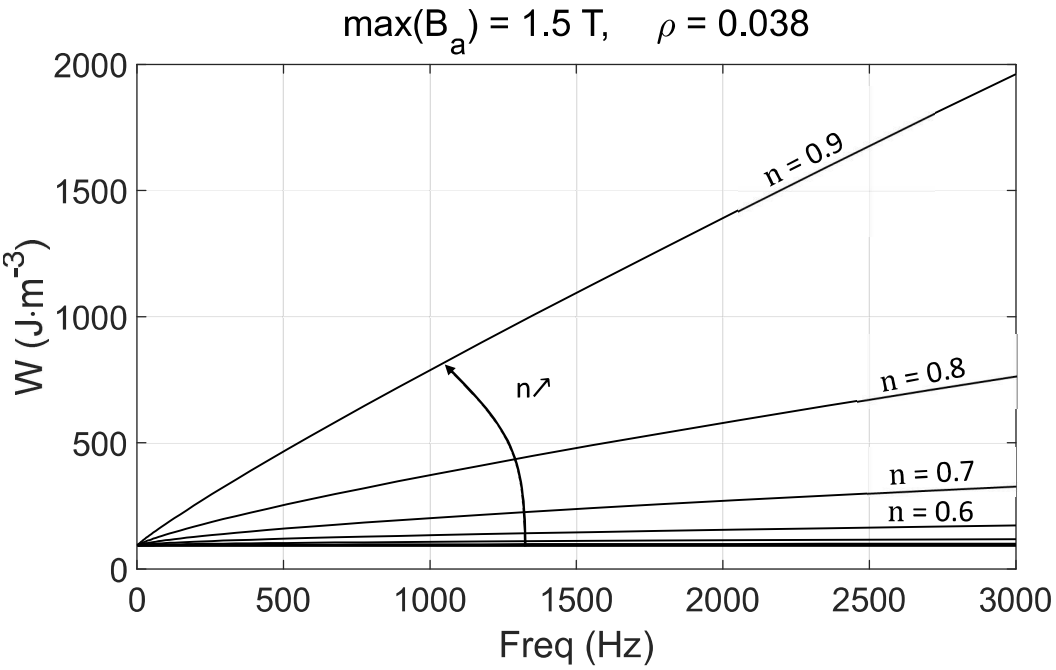

Fig. 4 Hysteresis core losses W simulation as a function of f under sinus B_a imposed condition using the fractional viscoelastic differential equation Eq. (9) for max(B_a) = 1.5 T, ρ = 0.038 and increasing n.

Fig. 3 shows the loss variations for increasing ρ, f, n, and max(B_a), and Fig. 4 the fractional-order influence for given ρ and max(B_a). ρ is set randomly to 0.038 and max(B_a) to 1.5 for comparison purposes [24]. Table 2 quasi-static parameters are considered for all these simulations.

B. The hybrid lump method

The resolution of Eq. (9) in sinus B_a imposed conditions is fast, simple, and provides flexible simulation results. Still, it is also restrictive as it limits the frequency dependence to a unique term. It indirectly supposes that W_{cl} and W_{ex} are equally affected by the frequency, which contradicts previous studies [49][50]. In [24], Liu et al. proposed a different approach to better adequate real-life observations. They suggested keeping W_{hy} and W_{ex} as described by STL and

restricting the use of the fractional viscoelastic term $\rho \cdot d^n B_a/dt^n$ to the only W_{cl} contribution. The resulting equation Eq. (13) remains simple as every element can be considered separately (Fig. 5), and excellent results are observed up to 3 kHz.

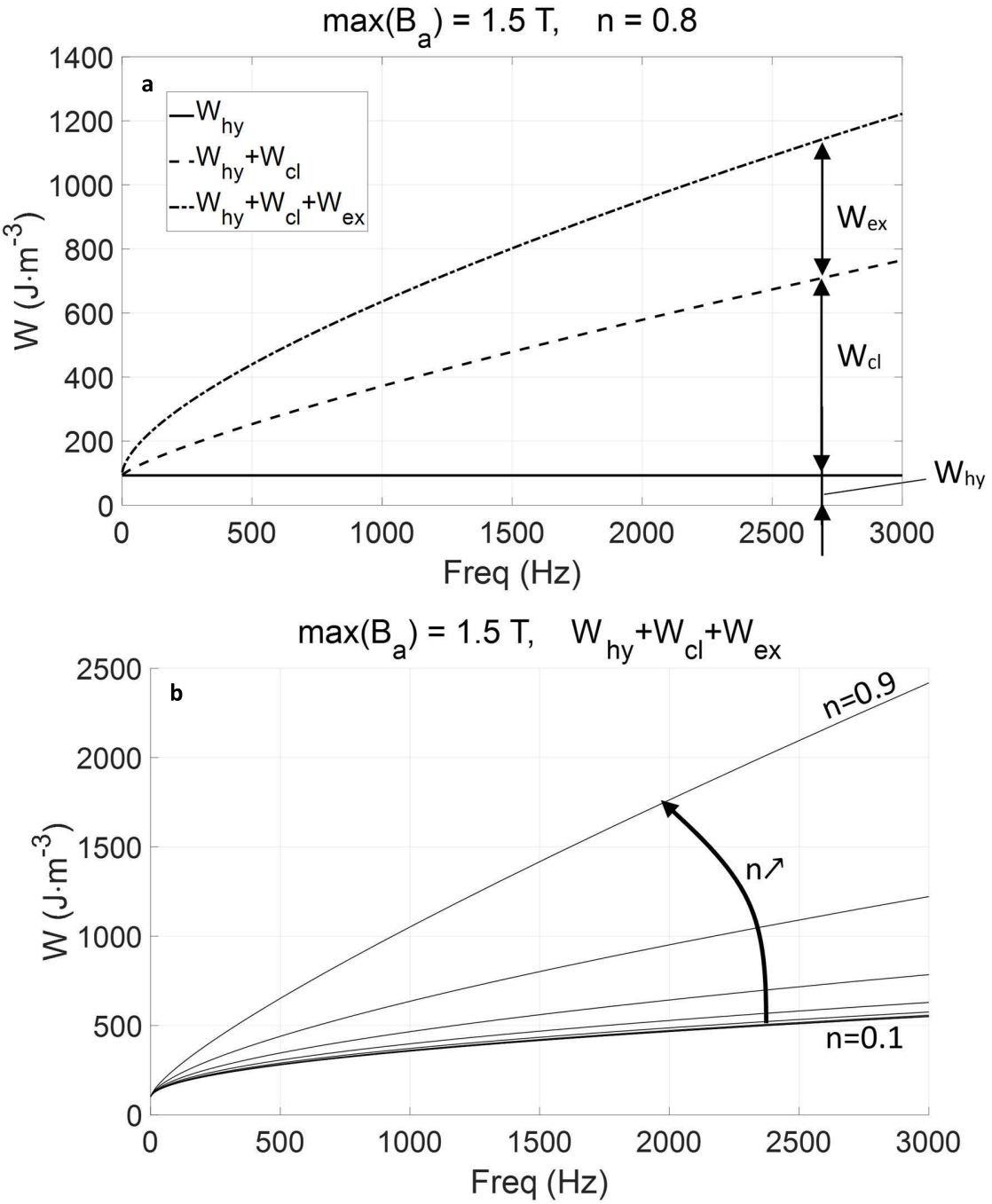

Fig. 5.a Hysteresis core losses distribution (W_{hy}, W_{cl} and W_{ex}) simulated under sinus B_a imposed condition using the hybrid method proposed in [24] for max(B_a) = 1.5 T, ρ = 0.038 and n = 0.8. W_{hy}, W_{ex} comes from [24]. **Fig. 5.b** Hysteresis core losses W variations under identical conditions for n € [0.1 - 0.9].

Unfortunately, compared to other methods, the capability of solving the time-dependent problem is lost. Fig. 5 – a depicts the hysteresis core losses distribution obtained by solving Eq. (13) under sinus flux density, max(B_a) = 1.5 T and n = 0.8. Fig. 5 – b shows the influence of n on the frequency dependence of W.

C. The fractional diffusion equation method

With Eq. (13), Liu et al. [24] have provided an excellent way to precisely simulate the magnetic losses on a considerable frequency bandwidth. The frequency impacts W_{cl} and W_{ex} differently, which agrees with STL. However, Eq. (13) remains a lumped-element method, and local information (distribution of H and B) is still unavailable. In [25][26], the authors proposed considering the magnetic losses differently. Their idea found its origin in the description of the classic losses as described by the Maxwell diffusion equation Eq. (5). In the low-frequency range, under sinus flux density imposed conditions, the resolution of this equation is supposed to give the same amount of losses as STL classic losses contribution (W_{cl}). This statement is verified in Fig. (6), where the classical hysteresis loss contribution is simulated from both the STL and the Maxwell expressions. The diffusion equation is solved in 1D using finite differences for the space term [27][48]-[52] and considering the lamination thickness and the space step equal to 0.2 mm and 0.002 mm, respectively (q = 100 nodes for the whole thickness).

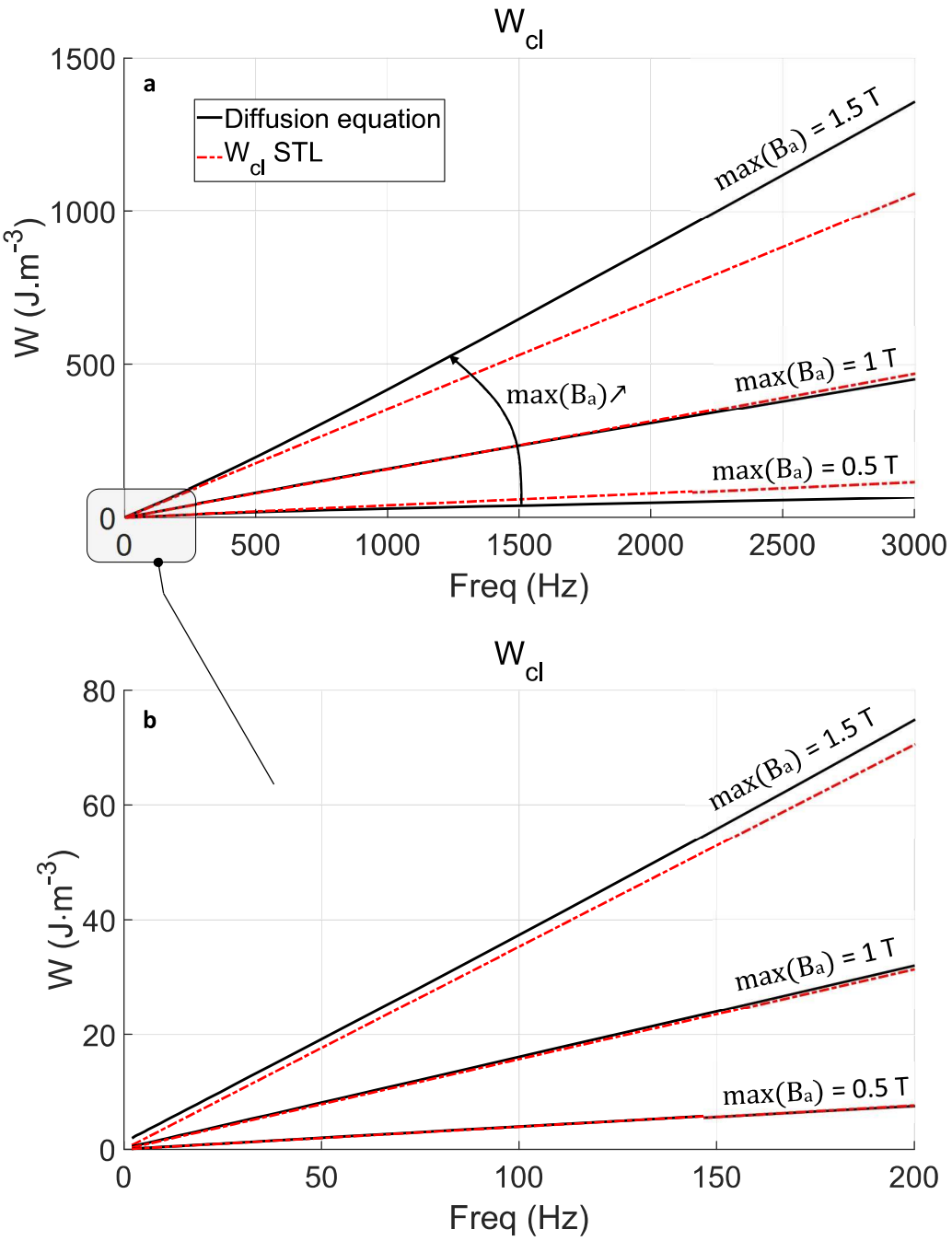

Fig. 6.a Comparison of the classic losses frequency dependence $W_{cl}(f)$ calculated using the STL expression and the 1D Maxwell diffusion equation. **Fig. 6.b** Same comparison in the low-frequency range.

The conductivity is set to 1.99 10^6 S·m^{-1}, like in [24]. The space discretization is homogeneous, and B_a is calculated by averaging the local magnetic values B_i :

$$B_a = \frac{\sum_{i=1}^{q} B(z)}{q} \tag{20}$$

Fig. 6 results confirm the excellent prediction of STL, especially in the low-frequency range where the complete flux penetration condition is valid. In the following figure, the classic diffusion equation is replaced by a fractional one as described in [27]. The fractional diffusion equation and the generalized fractional Maxwell equations [53] seem connected. Still, their relations need to be established. Even if the mathematical description of the fractional Maxwell equations has already been described in the literature [54], one may question the physical meaning of such description. Similar to complex mechanical media (fractal geometries, composites materials, etc. [54][55]), magnetization processes involve multi-scale interactions, although this parallel has not been addressed yet. Eq. (14) in sinus B_a imposed condition and max(B_a) = 1.5 T is solved explicitly with a limited tested window (+/- 3 A·m^{-1}) of H_{surf} centered around its value at t = t - dt. The finite differences are still used for the space term and the forward Grünwald-Letnikov Eq. (15) for the time-fractional derivative term. The time discretization is about 1000 points per period, and a complete hysteresis cycle is obtained in less than a minute. Besides the questionable physical origin of the fractional diffusion equation, another issue is noticed: a decrease of n reduces the losses.

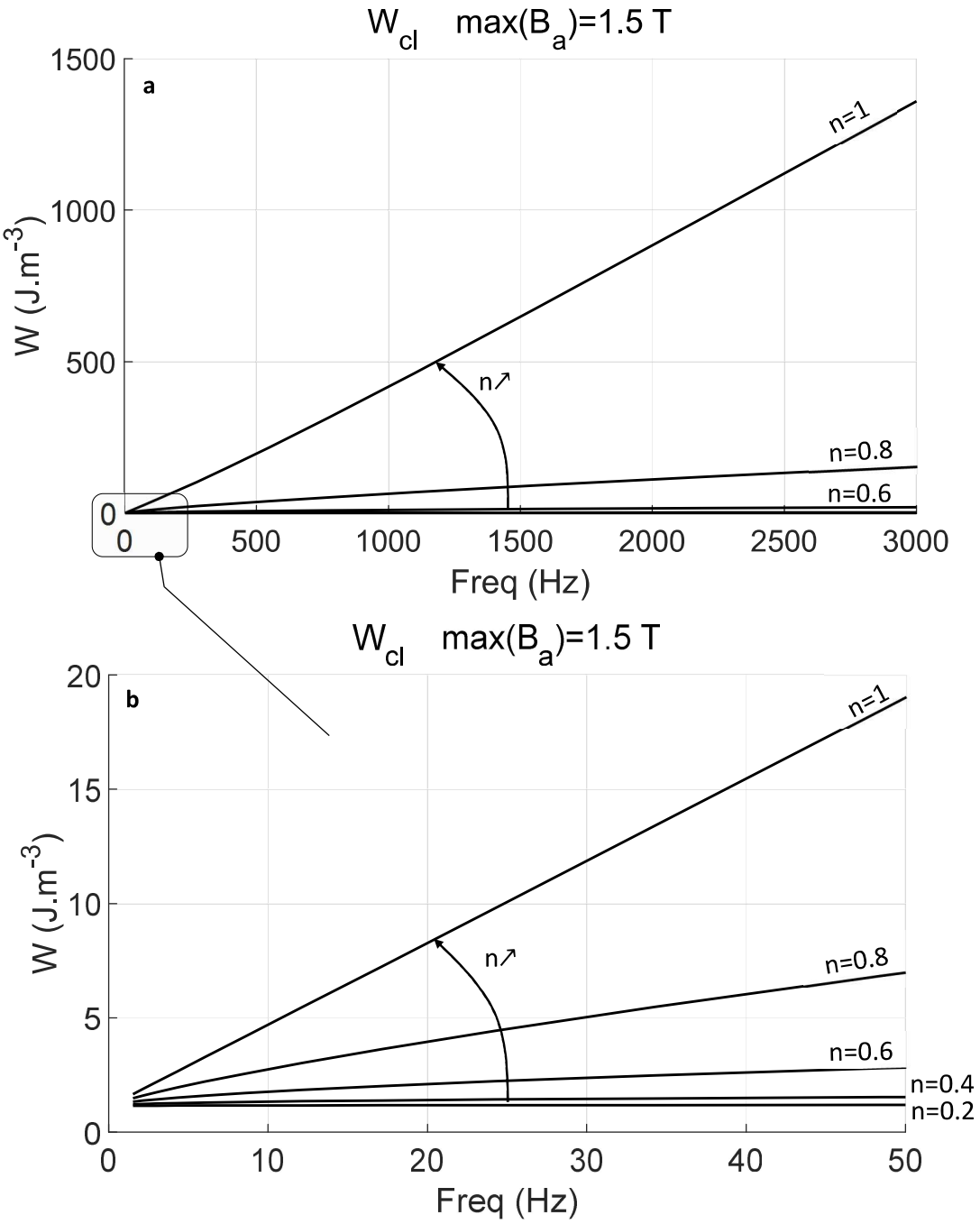

Fig. 7.a Classic hysteresis losses W_{cl} simulation as a function of f under sinus B_a imposed condition using the fractional diffusion equation (Eq. 13) and for $n \in [0.1 - 0.9]$. **Fig. 7.b** Same comparison in the low-frequency range.

As commented in the introduction, correct simulation results can only go through a wrong estimation of the electrical conductivity. A hybrid method like in 3.2, where the fractional diffusion equation would be restricted to the classic losses, can be considered and lead to the simulation results depicted in Fig. 8 below (like Fig. 5 – b, the flux density is imposed sinus and max(B_a) = 1.5 T). Similar trajectories are observed between Fig. 5 – b and Fig. 8. Still, the same values of n can lead to very different amounts of losses. In [24], the classic losses are weighted by ρ, and even in the low n range, high values of the classic losses can be obtained.

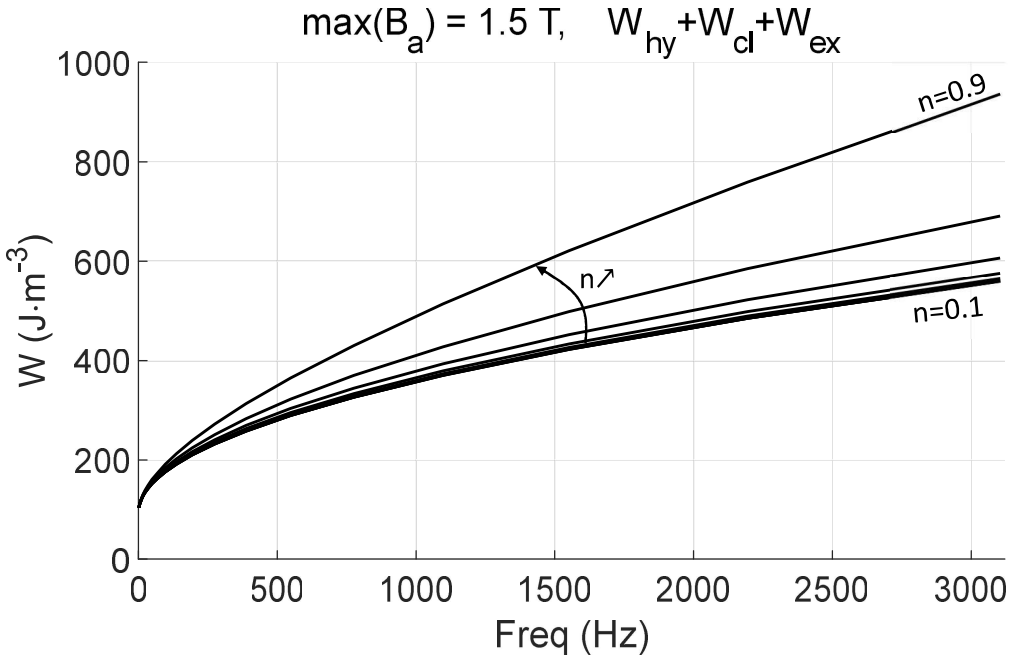

Fig. 8 Hysteresis core losses simulation as a function of f under sinus flux density imposed condition using the fractional diffusion equation method Eq. (13) and for n € [0.1 - 0.9].

D. Combination of the classical diffusion equation to a fractional material law

Like Eq. (5) and (6) are regrouped in (7), if n is similar in (9) and (14), a similar rearrangement can be applied :

$$\frac{d^n B(z,t)}{dt^n} = \frac{1}{\sigma}\frac{\partial^2 H(z,t)}{\partial z^2} = \frac{H(z,t) - {f_{static}}^{-1}(B(z,t))}{\rho} \tag{21}$$

Eq. (23) can be solved through matrix inversion (Euler's method) as described in [18]. For each simulation time step, the determination of local $H(z,t)$ is followed by a resolution of Eq. (24), leading to $B(z,t)$ for every node of the mesh:

$$B(z,t) = \frac{d^{-n}\left(\frac{H(z,t) - {f_{static}}^{-1}(B(z,t))}{\rho}\right)}{dt^{-n}} \tag{22}$$

This method is attractive, and its computation is straightforward. It provides local information and accurate simulation results. Still, the physical meaning of Eq. 14 and the associated fractional Maxwell equations remains unsolved. An even better approach starts from a reformulation of Eq. (9):

$$\frac{d^n B(z,t)}{dt^n} = \frac{H(z,t) - H_{stat}(B(z,t))}{\rho} \tag{9}$$

$$\frac{d^{1-n}}{dt^{1-n}}\left(\frac{d^n B(z,t)}{dt^n}\right) = \frac{d^{1-n}}{dt^{1-n}}\left(\frac{H(z,t) - H_{stat}(B(z,t))}{\rho}\right) \tag{9}$$

$$\left(\frac{dB(z,t)}{dt}\right) = \frac{d^{1-n}}{dt^{1-n}}\left(\frac{H(z,t) - H_{stat}(B(z,t))}{\rho}\right) \tag{9}$$

By isolating dB/dt this way, the concatenation with Eq. (6) is still possible and leads to Eq. (23):

$$\frac{1}{\sigma}\frac{\partial^2 H(z,t)}{\partial z^2} = \frac{d^{1-n}}{dt^{1-n}}\left(\frac{H(z,t) - H_{stat}(B(z,t))}{\rho}\right) \tag{23}$$

Euler's method (matrix inversion) is no more applicable, but the resolution describes in [25] is. The right term is expressed through the forward Grünwald-Letnikov expression Eq. (26), and the left term through finite differences. Fig. 9 depicts the space discretization and the boundary conditions.

$$\frac{\partial^2 H(z,t)}{\partial z^2} = \sigma \cdot \lim_{h \to 0^+} h^{n-1} \cdot \sum_{m=0}^{\infty} \frac{(n-1)m}{m!} \cdot \left(\frac{H(z,t-mh) - H_{stat}(B(z,t-mh))}{\rho} \right) \quad (24)$$

In this configuration, the matrix resolution is still possible, but the stiffness matrix needs to be recalculated at every step time. Once all $H(z,t)$ are obtained from the matrix resolution, Eq. (24) is applied to every node of the mesh leading to $B(z,t)$.

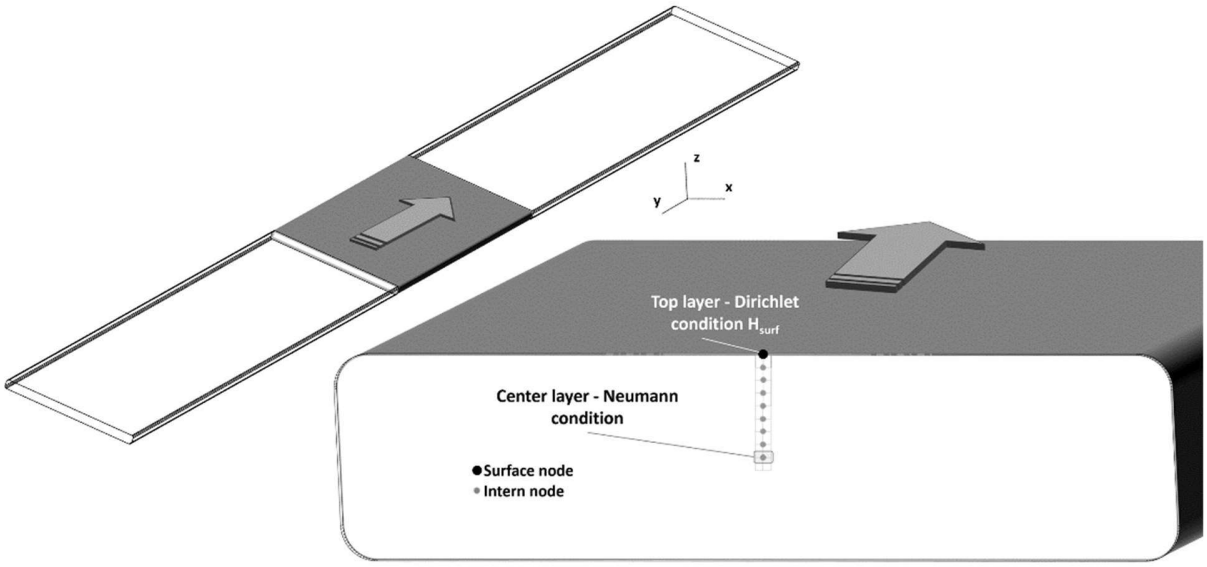

Fig. 9 1D space discretization resolution scheme, including the boundary conditions.

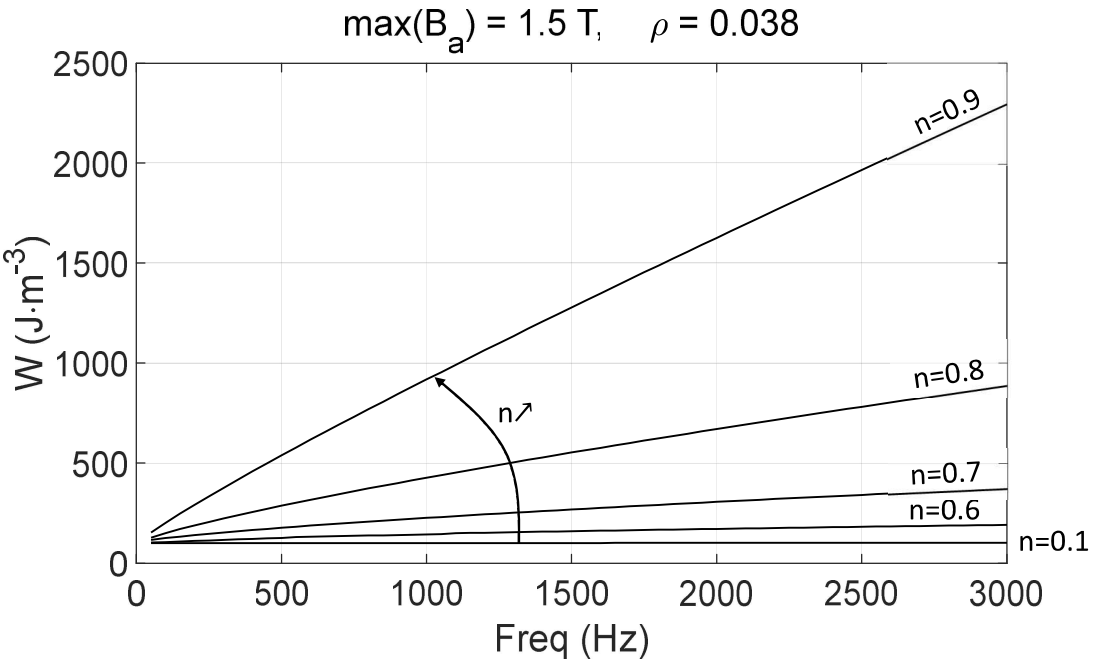

Fig. 10 Hysteresis core losses simulation as a function of f under sinus flux density imposed condition using the combination of the diffusion equation and the fractional material law, Eq. (26), and for n € [0.1 - 0.9].

Fig. 10 gives the core losses simulated with Eq. 26 in sinus B_a imposed condition and max(B_a) = 1.5 T. The explicit method is used again so are the J-A model and Table 2 parameters for the static contributions. Fig. 11 depicts B(z,t) and H(z,t) chronograms as obtained from the resolution of the method mentioned above and different values of n and frequencies. As anticipated, a significant skin effect can be observed at 200 Hz when n is high. Oppositely for low n, the magnetic behaviors of the top and center layers are confounded.

V. COMPARISONS TO EXPERIMENTAL RESULTS

The measurement methods of the magnetic core losses in a ferromagnetic lamination are described in international standards [56]-[58].

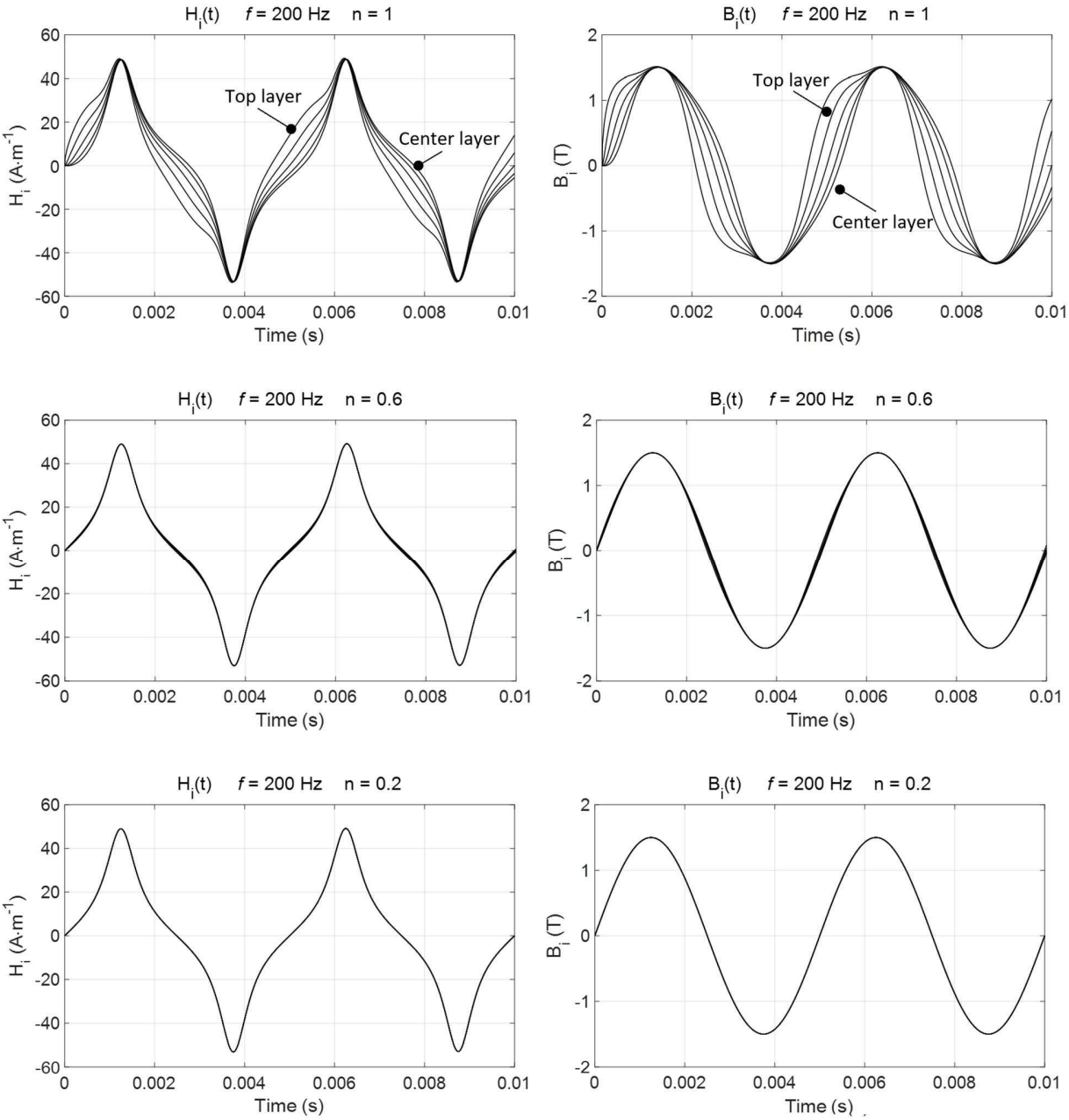

Fig. 11 $B_i(t)$ and $H_i(t)$ for f = 200 Hz and n = 1, 0.6 and 0.2 respectively.

For the Epstein frame method [57], the reproducibility standard deviation is 1.5% up to 1.5 T for non-oriented electrical steels and 1.7 T for oriented ones. Similarly, the reproducibility of the magnetic behavior of same-grade electrical steel is far from ensured by the manufacturer. In [59], for instance, the test values are supposed to be typical but not guaranteed. The accumulation of

the characterization setup and the specimen behavior uncertainties makes access to reliable and comparable experimental data hazardous. For these reasons, such as the fact that typical FeSi GO has been substantially studied and many convergent experimental data can be found in the literature, we used already published experimental results instead of carrying out a new testing campaign. In this section, all the experimental results came from [17][24] and [60][61]. The specimens tested were FeSi Go laminations of thickness 0.22 mm and conductivity 1.99 10^6 $S{\cdot}m^{-1}$. We refer readers to the original documents for additional information, including the experimental conditions. In Fig. 11 below, simulations and measurements are compared for increasing max(Ba) values. Concerning the simulations, three methods were tested:

_ the fractional differential equation method (sub-section 3.1),

_ the hybrid lump method (sub-section 3.2),

_ The combination of the diffusion equation and a fractional material law (sub-section 3.4).

The dynamic simulation parameters for the hybrid lump method were those of [24]. For both the other ways, they were set through the minimization of an uncertainty function:

$$\text{Uncertainty}\ (\%) = \frac{100}{\mathrm{p}} \cdot \sum_{\mathrm{i}=1}^{\mathrm{p}} \frac{\left|\mathrm{W}_{\mathrm{meas_i}} - \mathrm{W}_{\mathrm{sim_i}}\right|}{\mathrm{W}_{\mathrm{meas_i}}} \tag{25}$$

Where p is the time discretization's number, the static parameters came from Table 2. Table 3 gives the dynamic simulation parameters for the fractional differential equation and the diffusion equation/fractional material law methods. Eq. 24 gives the expression of V_0 (associated with Eq. 13) as a function of max($\mathrm{B_a}$) used for the hybrid lump method:

$$\mathrm{V}_0 = -0.076 \cdot \max\left(\mathrm{B_a}\right) + 0.25 \tag{26}$$

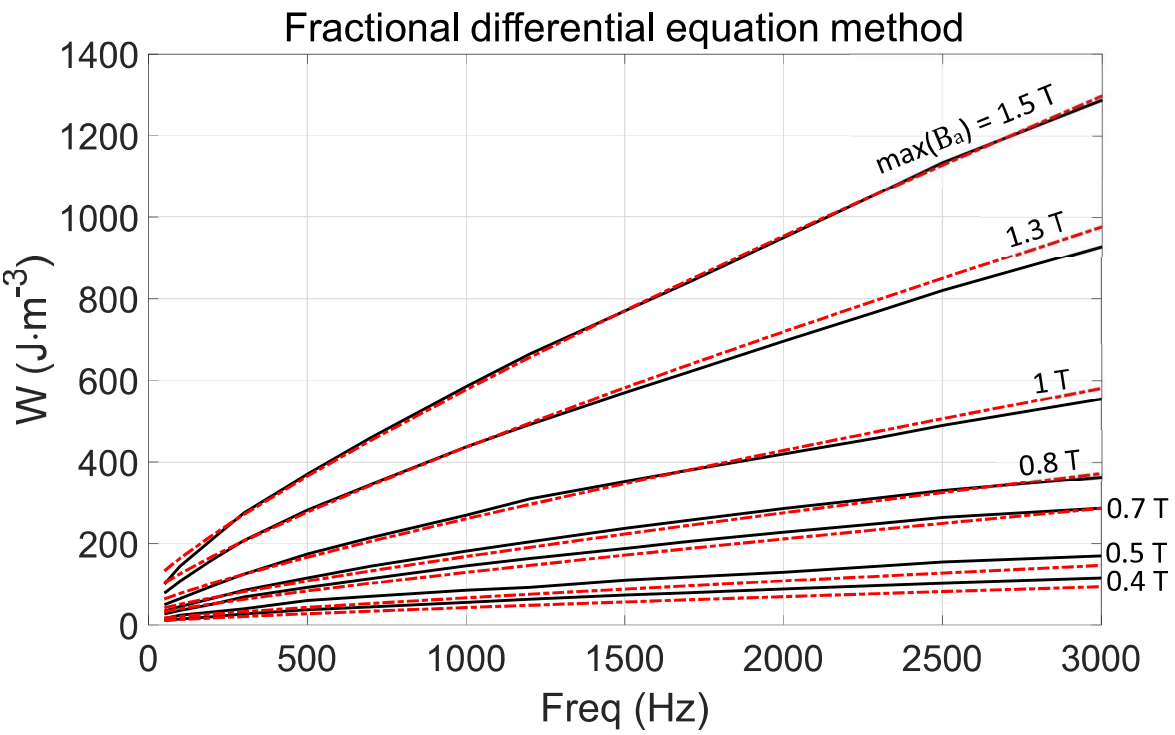
Fractional differential equation method
W (J·m-3)
Freq (Hz)
max(Ba) = 1.5 T
1.3 T
1 T
0.8 T
0.7 T
0.5 T
0.4 T
0
200
400
600
800
1000
1200
1400
0
500
1000
1500
2000
2500
3000

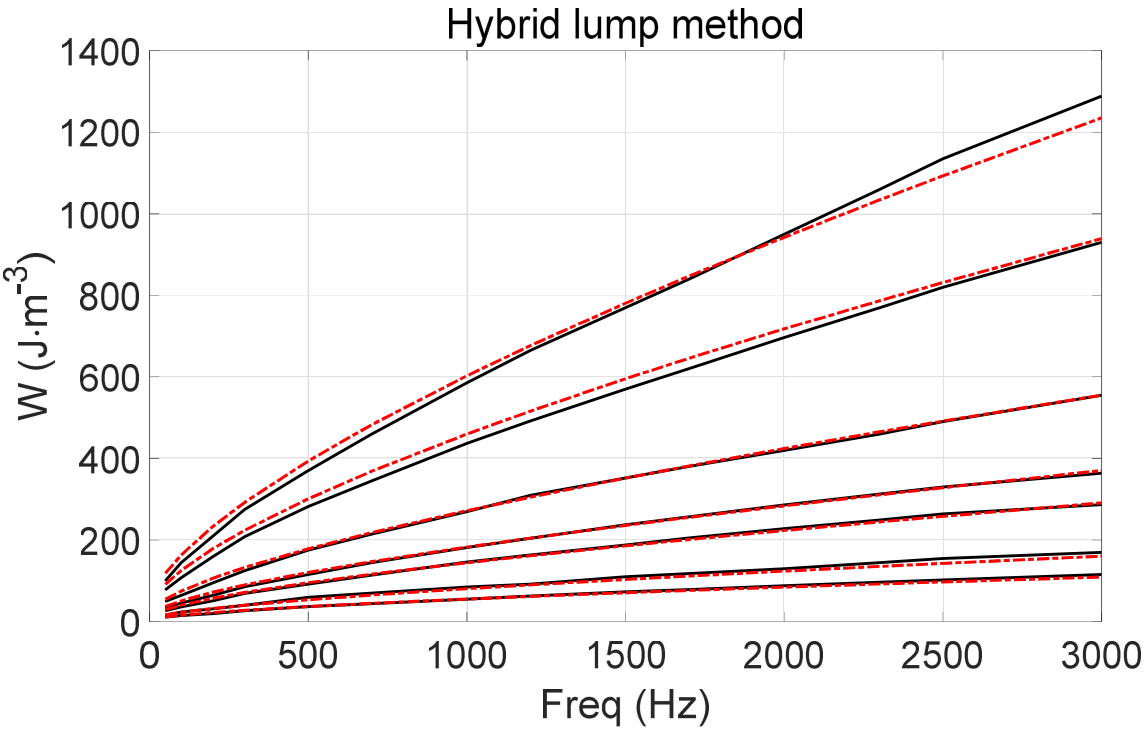
Hybrid lump method
W (J·m-3)
Freq (Hz)
0
200
400
600
800
1000
1200
1400
0
500
1000
1500
2000
2500
3000

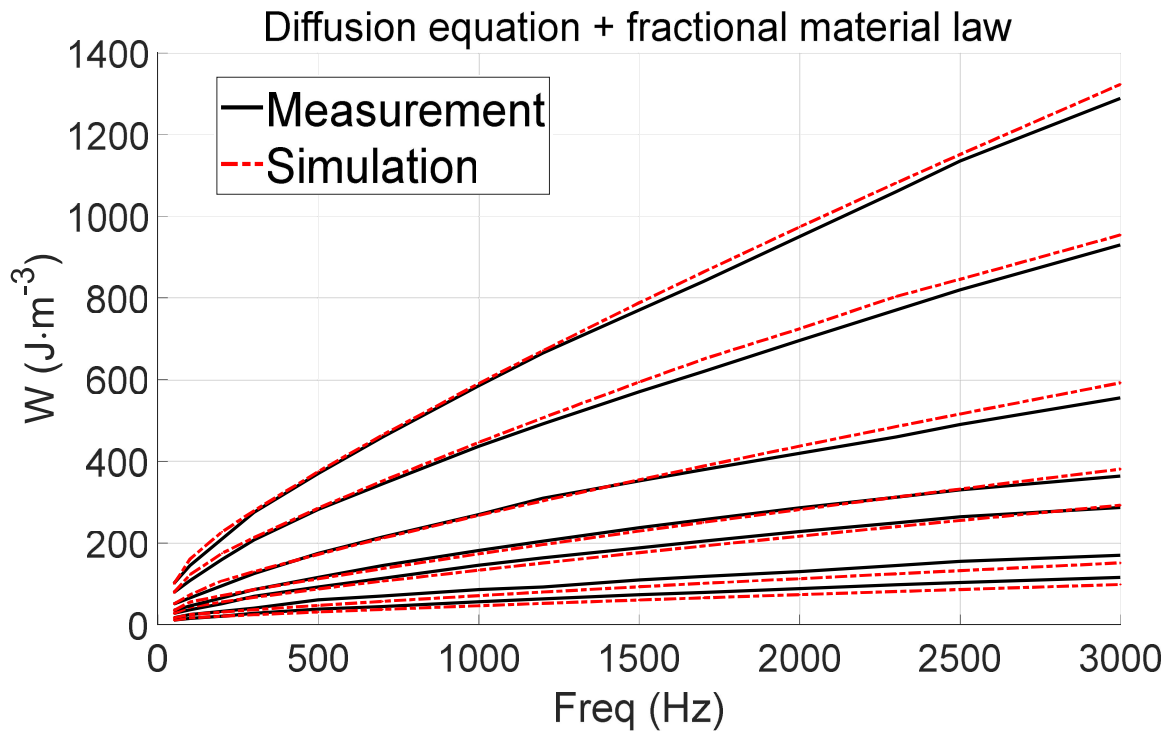

Fig. 12 Comparison simulations/experimental results for the three simulation methods.

TABLE III

Dynamic simulation parameters.

Fractional differential equation method:		**Diffusion equation + fractional material law method:**	
ρ	0.05	ρ	0.045
n	0.83	n	0.835

Table 4 depicts the simulation methods accuracy quantitatively, and Table 5 compared the methods regarding the criteria defined in Table 1 and the performances.

TABLE IV

Quantitative comparisons (uncertainty) for all Fig. 12 simulation tests.

Fractional differential equation method:

Freq (Hz)	**100**	**200**	**300**	**500**	**700**	**1000**	**1200**	**1500**	**1700**	**2000**	**2300**	**2500**	**3000**	**Uncertainty (%)**
B_{MAX} (T)														
0.4	10.1	13.6	22.6	26.4	23.1	23.1	23.3	22.7	21.3	21.1	20.6	20.1	19.0	20.58
0.5	13.7	15.9	18.6	28.3	24.6	21.7	18.1	19.9	18.3	16.6	17.1	17.5	13.7	18.79
0.7	10.1	1.55	8.86	9.36	10.0	11.2	10.2	8.66	8.34	7.21	5.78	5.42	0.15	7.47
0.8	12.2	2.96	4.78	6.73	8.17	7.19	6.62	5.86	4.79	3.81	2.17	1.39	2.63	5.33
1	19.3	7.74	0.00	4.66	4.26	3.33	4.46	1.39	0.03	2.00	3.36	3.32	4.77	4.52
1.3	17.0	5.14	0.73	1.70	0.54	0.15	0.77	2.08	2.84	3.34	3.74	3.76	5.16	3.61
1.5	13.4	4.85	1.41	1.28	1.51	1.34	1.31	0.12	0.61	0.40	0.03	0.53	0.79	2.12
Uncertainty (%)	13.73	7.41	8.15	11.21	10.33	9.74	9.27	8.68	8.05	7.78	7.55	7.43	6.61	8.92

Hybrid lump method:

Freq (Hz)	**100**	**200**	**300**	**500**	**700**	**1000**	**1200**	**1500**	**1700**	**2000**	**2300**	**2500**	**3000**	**Uncertainty (%)**
B_{MAX} (T)														
0.4	8.35	13.1	3.86	0.84	2.47	0.19	1.54	2.70	2.29	3.60	4.56	4.82	5.59	4.15
0.5	3.63	2.03	1.25	10.2	6.57	4.88	1.83	5.81	5.09	4.59	6.54	7.79	5.48	5.06
0.7	13.0	12.8	3.76	3.85	2.15	1.01	1.06	1.04	1.74	1.97	1.76	2.17	1.40	3.68
0.8	12.4	11.5	5.53	3.99	1.53	0.82	0.23	0.64	0.53	0.92	0.52	0.51	1.73	3.15
1	15.4	12.2	6.43	1.98	1.55	0.77	1.56	0.02	0.42	1.01	1.12	0.32	0.03	3.30
1.3	16.3	12.0	7.74	6.78	6.87	5.22	4.86	4.42	4.10	3.12	2.20	1.43	1.02	5.86
1.5	12.6	11.2	6.37	6.43	4.93	3.01	1.74	1.43	0.86	0.78	2.46	3.70	4.10	4.60
Uncertainty (%)	11.71	10.73	4.99	4.88	3.73	2.27	1.83	2.29	2.15	2.29	2.74	2.96	2.76	4.26

Diffusion equation + fractional material law method:

Freq (Hz)	**100**	**200**	**300**	**500**	**700**	**1000**	**1200**	**1500**	**1700**	**2000**	**2300**	**2500**	**3000**	**Uncertainty (%)**
B_{MAX} (T)														
0.4	9.02	0.79	11.8	18.3	16.1	17.3	18.1	18.1	17.0	17.0	16.9	16.5	15.7	14.85
0.5	0.22	5.47	9.87	22.2	19.2	17.1	13.7	16.1	14.7	13.2	13.9	14.5	10.8	13.19
0.7	18.6	7.98	4.01	5.40	6.71	8.43	7.56	6.14	5.95	4.92	3.59	3.26	2.00	6.51
0.8	20.0	8.67	0.29	3.12	5.02	4.41	4.04	3.50	2.50	1.62	0.03	0.69	4.68	4.51
1	11.1	12.8	4.20	1.42	1.40	0.82	2.12	0.84	2.17	4.10	5.42	5.30	6.71	4.50
1.3	13.2	9.31	2.72	1.23	2.07	2.15	2.99	4.18	4.84	4.12	4.30	3.13	2.59	4.38
1.5	10.7	8.27	1.52	1.41	0.98	0.98	0.92	2.31	2.75	2.49	1.99	1.43	2.70	2.96
Uncertainty (%)	11.88	7.63	4.93	7.61	7.37	7.32	7.08	7.32	7.13	6.79	6.60	6.41	6.47	7.27

TABLE V

Simulation methods vs. comparison criteria

	Simulation method		
Comparison criteria	Fractional differential equation	Hybrid lump method	Diffusion equation + fractional material law
Core loss (harmonic regime)	+ +	+ +	+ +
Core loss (transient regime)	+	- -	+ +
Spatial distribution	- -	- -	+ +
Simulation speed	+	+ +	0
Number of parameters	+ +	-	+

Simulation objectives Performance criteria

As illustrated in Fig. 11 and observed in Table 4, an average precision of less than 10 % can be obtained with the three methods tested. The Hybrid lump and the fractional diffusion equation methods show accuracy levels close to 5 %, but four parameters (two for V_0, ρ, and n) are necessary for the first method while only two are used by the second (ρ, and n).

Finally, under the same model settings conditions, the diffusion equation + fractional material law speed is approximately 200 times slower than the other methods. However, with around 30 seconds per period, the simulation time remains reasonable and should not constitute a reason to discriminate against this method.

VI. CONCLUSION

The problem of magnetic losses in laminated electrical steel sheets is constantly evolving. Old-fashion, low-frequency, high-power transformers still exist. Still, new designs of improved performances and working frequencies up to fifty times higher than the distribution frequency

are frequently seen nowadays. Former simulation tools like STL, adapted to the end of the 20th-century electromagnetic environment, show limitations in this contemporary context. This manuscript reviewed and studied alternative methods based on fractional derivatives operators. Comparisons with experimental observations confirmed that the fractional derivative methods could obtain accurate results on large frequency bandwidths.

On the one hand, the fractional differential equation method is simple to solve as an analytical solution is available under sinus B imposed experimental conditions. On the other hand, the well-admitted loss separation is impossible with a unique frequency-dependent contribution. The hybrid method combining STL for the hysteresis and the excess losses to a fractional derivative term for the classic ones is consistent as it respects the separation principle. It is simple to solve as each contribution can be calculated separately, but it can't provide local information like the skin effect. The combination of the diffusion equation with a fractional material law was the last option proposed in this study. Good accuracy was observed again. Once the electrical conductivity is known, its implementation is easy as it relies on only a few parameters (ρ and n). Furthermore, it gives access to local information, skin effect, etc. Concerning the simulation speeds, the fractional differential equation and the hybrid method are extremely fast. No iterative loops are necessary, and the simulation times are mainly due to the initialization of the parameters and the results' plots. The combination diffusion equation + fractional material law method is definitively more demanding of computation time and numerical resources. However, the simulation speed remains reasonable with less than a minute per period using a standard computer. In this study, all tests and simulations were done following the rules of the characterization standards. We know that the frequency effects can be observed

differently in domains like magnetic non-destructive testing (incremental permeability, impedance spectroscopy, etc.). In the perspective of this study, tests will be done to check the viability of the proposed method under these alternative experimental situations. The highest frequency tested has been arbitrarily set to 3 kHz; still, it would be of significant interest to get comparisons up to 10 kHz.

REFERENCES

[1] F. Bitter, “On inhomogeneities in the magnetization of ferromagnetic materials,” *Phys. Rev.,* 38, pp. 1903, 1931.

[2] P. Weiss, “L’hypothèse du champ moléculaire et le propriété ferromagnétique,” *J. de Phys.*, vol. 6, pp. 661 – 690, 1907.

[3] C.S. Schneider, S.D. Gedney, N. Ojeda-Ayala, M.A. Travers, “Dynamic exponential model of ferromagnetic hysteresis,” *Phys. B: Cond. Mat.*, vol. 607, 412802, 2021.

[4] H. Zhao, H.H. Eldeeb, Y. Zhang, Y. Zhang, G. Xu, O.A. Mohammed, “An improved core loss model of ferromagnetic materials considering High-frequency and non-sinusoidal supply,” *2020 IEEE Ind. App. Soc. Ann. Meet.*, 10 – 16 Oct. 2020, Detroit, MI, USA.

[5] A. Magni, A. Sola, O. de la Barrière, E. Ferrara, L. Martino, C. Ragusa, C. Appino and F. Fiorillo, “Domain structure and energy losses up to 10kHz in grain-oriented Fe-Si sheets,” *AIP Advances* 11, 015220, 2021.

[6] R. Corcolle, X. Ren, L. Daniel, “Effective properties and eddy current losses of soft magnetic composites,” *J. Appl. Phys.*, vol. 129, 015103, 2021.

[7] F.J.G. Landgraf, C. Ragusa, D.L.R. Junior, M.B.S. Dias, O. de la Barrière, F. Mazaleyrat, F. Fiorillo, C. Appino, L. Martino, “Loss decomposition in plastically deformed and partially annealed steel sheets,” *J. of Mag. and Mag. Mat.*, vol. 502, 166452, pp. 212-221, 2020.

[8] M. S. Lancarotte, C. Goldemberg, A. d. A. Penteado, “Estimation of FeSi Core Losses Under PWM or DC Bias Ripple Voltage Excitations, ” *IEEE Trans. on Ener. Conv.*, vol. 20, no. 2, pp. 367-372, June 2005.

[9] T. L. Mthombeni, P. Pillay, R. M. W. Strnat, "New Epstein Frame for Lamination Core Loss Measurements Under High Frequencies and High Flux Densities," *IEEE Trans. on Ener. Conv.*, vol. 22, no. 3, pp. 614-620, 2007.

[10] M. S. Lancarotte, A. de A. Penteado, “Estimation of core losses under sinusoidal or nonsinusoidal induction by analysis of magnetization rate, ” *IEEE Trans. on Ener. Conv.*, vol. 16, no. 2, pp. 174-179, June 2001, doi: 10.1109/60.921469.

[11] C.P. Steinmetz, “On the law of hysteresis,” *AIEE Trans.*, vol. 9, pp. 3 – 64, 1892. Reprinted under the title “A Steinmetz contribution to the AC power revolution,” Introduction by J.E. Brittain, *Proc. IEEE*, vol. 72, n° 2, pp. 196 – 221, 1984.

[12] F.J.G. Landgraf, M. Emura, M.F. de Campos, “On the Steinmetz hysteresis law,” *J. of Mag. and Mag. Mat.*, Vol. 329, Iss. 20, pp. 531-534, 2008.

[13] L. Petrescu, V. Ionita, E. Cazacu, C. Petrescu, "Steinmetz' parameters fitting procedure for the power losses estimation in soft magnetic materials," *2017 Int. Conf. on Optimization of Electrical and Electronic Equipment (OPTIM) & 2017 Int. Aegean Conf. on Electrical Machines and Power Electronics (ACEMP),* pp. 208 – 213, 2017.

[14] J. Reinert, A. Brockmeyer, R. W. A. A. De Doncker, "Calculation of losses in ferro and ferrimagnetic materials based on the modified Steinmetz equation," *IEEE Trans. Ind. App.,* vol. 37, n° 4, pp. 1055 – 1061, 2001.

[15] G. Bertotti, “General properties of power losses in soft ferromagnetic materials, ” *IEEE Trans. Magn.*, vol. 24, n° 1, pp. 621 – 630, 1988.

[16] G. Bertotti, “Hysteresis in Magnetism,” San Diego, CA, USA: Academic, 1998.

[17] A. Broddefalk, M. Lindenmo, “Dependence of the power losses of a non-oriented 3% Si-steel on frequency and gaude,” *J. of Mag. and Mag. Mat.*, Vol. 304, pp. 586-588, 2006.

[18] S.E. Zirka, Y.I. Moroz, P. Marketos, A.J. Moses, “Viscosity-based magnetodynamic model of soft magnetic materials,” *IEEE Trans. Magn.*, vol. 42, n° 9, pp. 2121 – 2132, 2006.

[19] M.A. Raulet, B. Ducharne, J.P. Masson and G. Bayada, “The magnetic field diffusion equation including dynamic hysteresis: a linear formulation of the problem,” *IEEE Trans. Magn.*, vol. 40, n° 2, pp. 872 – 875, 2004.

[20] S. Zhang, B. Ducharne, T. Uchimoto, A. Kita, Y.A. Tene Deffo, “Simulation tool for the Eddy Current Magnetic Signature (ECMS) non-destructive testing method,” *J. of Mag. and Mag. Mat.*, Vol. 513, 167221, 2020.

[21] S.E. Zirka, Y.I. Moroz, P. Marketos, A.J. Moses, D.C. Jiles, T. Matsuo, “Generalization of the classical method for calculating dynamic hysteresis loops in grain-oriented electrical steels,” *IEEE Trans. Magn.*, vol. 44, n° 9, pp. 2113 – 2125, 2008.

[22] B. Zhang, B. Gupta, B. Ducharne, G. Sebald, T. Uchimoto, “Preisach’s model extended with dynamic fractional derivation contribution,” *IEEE Trans. Magn.*, Vol. 54, n° 3, pp. 1 – 4, 2018.

[23] B. Zhang, B. Gupta, B. Ducharne, G. Sebald, T. Uchimoto, “Dynamic magnetic scalar hysteresis lump model, based on Jiles-Atherton quasi-static hysteresis model extended with dynamic fractional derivative contribution,” *IEEE Trans. Magn.*, vol. 54, n° 11, pp. 1 – 4, 2018.

[24] R. Liu, L. Li, "Analytical prediction of energy losses in soft magnetic materials over broadband frequency range," *IEEE Trans. Power Electron*., vol. 36, n° 2, pp. 2009 – 2017, 2021.
[25] B. Ducharne, Y.A. Tene Deffo, B. Zhang, G. Sebald, "Anomalous fractional diffusion equation for magnetic losses in a ferromagnetic lamination," *The European Physical Journal Plus*, 135:325, 2020.
[26] B. Ducharne, P. Tsafack, Y.A. Tene Deffo, B. Zhang, G. Sebald, "Anomalous fractional magnetic field diffusion through the cross-section of a massive toroidal ferromagnetic core," *Com. in Nonlin. Sci. and Num. Sim*., vol. 92, 105450, 2020.
[27] B. Ducharne, P. Tsafack, Y.A. Tene Deffo, B. Zhang, G. Sebald, "Fractional operators for the magnetic dynamic behavior of ferromagnetic specimens: An overview," *AIP Advances* 11, 035309, pp. 1 – 6, 2021.
[28] S. Patnaik, J.P. Hollkamp, F. Semperlotti, "Applications of variable-order fractional operators: a review," *Proc. R. Soc. A*.476: 20190498, 2020.
[29] S.G. Samko, A.A Kilbas, O.I. Marichev, "Fractional integrals and derivatives. Theory and Applications," *Gordon and Breach Sc. Publ*., London, 1993.
[30] A.A. Kilbas, H.M. Srivastava, J.J. Trujillo, "Theory and applications of fractional differential equations," *Elsevier*, Amsterdam, 2006.
[31] M.D. Ortigueira, "Fractional calculus for scientists and engineers," *lecture notes in Electrical Engineering*, 84, Springer, Dordrecht, 2011.
[32] I. Petras, R.L. Magin, "Simulation of drug uptake in a two compartmental fractional model for a biological system," *Commun. Nonlinear Sci. Numer. Simulat.*, vol. 16, iss. 12, pp. 4588 – 4595, 2011.
[33] J.A.T. Machado, "And I say to myself: What a fractional world!," *Fract. Calc. and App. Anal.,* vol. 14, 635, 2011.
[34] X-J. Yang, J.A.T. Machado, C. Cattani, F. Gao, "On a fractal LC-electric circuit modeled by local fractional calculus," *Commun. Nonlinear Sci. Numer. Simulat.*, vol. 47, pp. 200 – 206, 2017.
[35] M.D. Ortigueira, J.A.T. Machado, "On fractional vectorial calculus," *Bulletin of the polish academy of sciences,* vol. 66, n° 4, pp. 389 – 402, 2018.
[36] G. Calcagni, "Geometry of fractional spaces," *Adv. Theor. Math. Phys.,* vol. 16, pp. 549 – 644, 2012.
[37] M. Ostoja-Starzewski, "Continuum mechanics models of fractal porous media: Integral relations and extremum principles," *J. of Mech. of Mat. and Struct.,* vol. 4, iss. 5, pp. 901 – 912, 2009.
[38] F. Mainardi, "Fractional calculus and waves in linear viscoelasticity: an introduction to mathematical models," Imperial College Press, 2010.
[39] R.L. Magin, C. Ingo, L. Colon-perez, W. Triplett, T.H. Mareci, "Characterization of anomalous diffusion in porous biological tissues using fractional order derivatives and entropy," *Mic. and Mes. Mat.,* vol. 178, pp. 39 – 43, 2013.
[40] B. C. Dos Santos, S. M. Oliva, J.D. Rossi, "A local/nonlocal diffusion model," *App. Anal.,* pp. 1 – 35, 2021.
[41] E.C. de Oliveria, J.A.T. Machado, "A review of definitions for fractional derivatives and Integral," Mathematical problems in engineering, article ID 238459, vol. 2014.
[42] S. Steentjes, F. Henrotte, K. Hameyer, "Energy-based ferromagnetic material model with magnetic anisotropy," *J. Magn. Magn. Mater.,* vol. 425, pp. 20 – 24, 2017.
[43] B. Ducharne, D. Guyomar, G. Sebald, "Low frequency modelling of hysteresis behaviour and dielectric permittivity in ferroelectric ceramics under electric field," *J. Phys. D: App. Phys.,* Vol. 40, Iss. 2, pp. 5511 – 555, 2007.
[44] J. V. Leite, N. Sadowski, P. Kuo-Peng, N. J. Batistela, J. P. A. Bastos, "The inverse Jiles-Atherton model parameters identification," *IEEE Trans. Magn.,* vol. 39, no. 3, pp. 1397 – 1400, 2003.
[45] R.-A. Naghizadeh, B. Vahidi, S. H. Hosseinian, "Parameter identification of Jiles-Atherton model using SFLA," *COMPEL,* vol. 31, iss. 4, pp. 1293 – 1309, 2012.
[46] H. Zhao, C. Ragusa, C. Appino, O. de la Barrière, Y. Wang, F. Fiorillo, "Energy losses in soft magnetic materials under symmetric and asymmetric induction waveforms," *IEEE Trans. Power Electron.,* vol. 34, no. 3, pp. 2655 – 2665, 2019.
[47] H. Zhao, C. Ragusa, O. de la Barrière, M. Khan, C. Appino, F. fiorillo, "Magnetic loss versus frequency in non-oriented steel sheets and its prediction: minor loops, PWM, and the limits of the analytical approach," *IEEE Trans. Magn.,* vol. 53, n° 11, pp. 1 – 4, 2017.
[48] B. Ducharne, G. Sebald, D. Guyomar, G. Litak "Dynamics of magnetic field penetration into soft ferromagnets," *J. App. Phys.,* 243907, pp. 1 – 9, 2015.

[49] B. Ducharne, G. Sebald, D. Guyomar, G. Litak, “Fractional model of magnetic field penetration into a toroidal soft ferromagnetic sample,” *Int. J. of Dyn. And Cont.,* pp. 1 – 8, 2017.
[50] M. Petrun, S. Steentjes, “Iron-loss and magnetization dynamics in non-oriented electrical steel: 1-D Excitations up to high frequencies,” *IEEE Access,* vol. 8, pp. 4568 – 4593, 2020.
[51] M. Petrun, S. Steentjes, K. Hameyer, D. Dolinar, “1-D lamination models for calculating the magnetization dynamics in non-oriented soft magnetic steel sheets,” *IEEE Trans. Magn.,* vol. 52, n° 3, 7002904, 2016.
[52] S.E. Zirka, Y.I. Moroz, S. Steentjes, K. Hameyer, K. Chwastek, S. Zurek, R.G. Harrison, “Dynamic magnetization models for soft ferromagnetic materials with coarse and fine domain structure,” *J. Magn. Magn. Mater.,* vol. 394, Iss. 15, pp. 229 – 236, 2008.
[53] M.D. Ortigueira, M. Rivero, J.J. Trujillo, “From a generalised Helmholtz decomposition theorem to fractional Maxwell equations,” *Commun. Nonlinear Sci. Numer. Simulat.*, vol. 22, pp. 1036 – 1049, 2015.
[54] V.E. Tarasov, “Fractional vector calculus and fractional Maxwell’s equation,” *Annals of Physics,* Vol. 323, Iss. 11, pp. 2756 – 2778, 2008.
[55] S. Patnaik, J.P. Hollkamp, F. Semperlotti, “Applications of variable-order fractional operators: a review,” *Proc. R. Soc. A*.476: 20190498, 2020.
[56] IEC 60404-3, “Magnetic materials – Part 3 : Methods of measurement of the magnetic properties of electrical steel strip and sheet by means of a single sheet tester,” International Electrotechnical Commission, 2010.
[57] IEC 60404-2, “Magnetic materials – Part 2 : Methods of measurement of the magnetic properties of electrical steel strip and sheet by means of an Epstein frame,” *International Electrotechnical Commission*, 2008.
[58] B. Koprivica, A. Milovanovic, M. Plazinic, “Standard Methods of Measurement of the Magnetic Properties of Electrical Steel Strip and Sheet,” *XI International SAUM Conference on Systems*, Automatic Control and Measurements Nis, Serbia, Nov 14th – 16th, 2012.
[59] “FJE steel corporation catalogue: Electrical steel sheets JFE G-CORE, JFE N-CORE,” Japan, 2003.
[60] Y. Zhang, M. C. Cheng and P. Pillay, “A Novel Hysteresis Core Loss Model for Magnetic Laminations,” *IEEE Trans. on Ener. Conv.*, vol. 26, no. 4, pp. 993-999, 2011.
[61] S. Yue, P. I. Anderson, Y. Li, Q. Yang and A. Moses, "A Modified Inverse Vector Hysteresis Model for Nonoriented Electrical Steels Considering Anisotropy for FEA,” *IEEE Trans. on Ener. Conv.*, vol. 36, no. 4, pp. 3251-3260, Dec. 2021.